Laminated TaS$_2$/Polymer Nanocomposites through Encapsulative Precipitation of Exfoliated Layers

Lei Wang and Mercouri G. Kanatzidis*

Department of Chemistry, Michigan State University, East Lansing, Michigan 48824

Received February 2, 2001

Several TaS$_2$/polymer nanocomposites prepared through the encapsulative precipitation method are described. Namely, the encapsulation of poly(ethylene oxide) (PEO), polyethylene imine (PEI), and poly(vinylpyrrolidinone) (PVP) into TaS$_2$ was examined in detail, and the nanocomposites were characterized by a wide variety of techniques. The nanocomposites disperse in water and are easily cast into free-standing films. The flexible metallic TaS$_2$/polymer nanocomposite films display bulk superconductivity. In addition, in this work the exfoliation properties of Li$_x$TaS$_2$ were systematically explored, and it was found that material prepared from controlled lithiation with 0.2 equiv of LiBH$_4$ exfoliates well in water and has high affinity for various polymers. The likely conformation of PEO molecules sandwiched between the TaS$_2$ slabs was explored with analysis of the X-ray diffraction patterns of a highly oriented Li$_x$(PEO)$_y$TaS$_2$ nanocomposite films. The one-dimensional electron density maps, obtained for Li$_x$(PEO)$_y$TaS$_2$, can be explained with two sheets of PEO chains (bilayer) that adopt a conformation similar to that found in a type II PEO−HgCl$_2$ complex. The chains are arranged with the −CH$_2$− groups facing the TaS$_2$ layers and the −O− atoms toward the center of the gallery, where the Li$^+$ ions seem to be located. Solid state ^{7}Li NMR measurements indicate that Li$_x$(PEO)$_y$TaS$_2$ provides a more facile hopping environment for Li ions than pristine Li$_x$TaS$_2$.

Introduction

Low-dimensional inorganic/polymeric nanocomposites represent an important and growing class of hybrid materials with promising physical properties. The research and development activity is concentrated mainly in two major fields, nanocomposites as structural materials[1] and as electroactive materials.[2,3] To synthesize laminated nanocomposites, the insertion of polymers in the galleries of layered hosts is the critical step. Polymer chains can be placed between the slabs of the layered materials through one of four major approaches: (a) by monomer intercalation and subsequent polymerization in the galleries, (b) by in situ redox intercalative polymerization, (c) by direct polymer insertion, and (d) by encapsulative precipitation of polymers from solutions of exfoliated lamellar solids. The latter two methods use preformed polymers and are capable of producing large varieties of materials. The direct polymer insertion approach works well with organically

modified clays.[1] On the other hand, the encapsulative precipitation method, which has been developed in our laboratory, has been successful in making nanocomposites with electroactive layered hosts.[4] In this method, the host exfoliates to give monolayers in solution, which interact with dissolved polymer chains and encapsulate them during a restacking process. This approach has led to the synthesis of various nanocomposites of MoS$_2$,[4a] MoO$_3$,[4b,5] NbSe$_2$,[4c] RuCl$_3$,[6] MoSe$_2$,[7] TiS$_2$,[8a] TaS$_2$,[8] and MPS$_3$.[8b,9]

The exfoliation behavior of TaS$_2$ has long been known,[10−12] and cations of many sizes have been encapsulated between the layers of this material. Early work in this area showed that electrochemically pre-

(1) *Adv. Mater.* **1996**, *8*, 29. (b) Krishnamoorti, R.; Vaia, R. A.; Giannelis, E. P. *Chem. Mater.* **1996**, *8*, 1728. (c) Fischer H. R., Gielgens L. H., Koster T. P. M. *Acta Polym.* **1999**, *50* (4), 122. (d) Carrado K. A. *Appl. Clay Sci.* **2000**, *17* (1−2), 1. (e) Zanetti, M.; Lomakin, S.; Camino, G. *Macromol. Mater. Eng.* **2000**, *279* (6), 1.

(2) (a) Pomogailo, A. D. *Russ. Chem. Rev.* **2000**, *69*, 53. (b) Ruiz-Hitzky, E. *Adv. Mater.* **1993**, *5*, 334. (b) Ruiz-Hitzky, E.; Aranda, P.; Casal, B.; Galván, J. C. *Adv. Mater.* **1995**, *7*, 180. (c) Oriakhi C. O. *J. Chem. Educ.* **2000**, *77*, 1138. (d) Oriakhi, C. *Chem. Br.* **1998**, *34* (11), 59.

(3) (a) Kanatzidis, M. G.; Tonge, L. M.; Marks, T. J.; Marcy, H. O.; Kannewurf, C. R. *J. Am. Chem. Soc.* **1987**, *109*, 3797. (b) Wu, C.-G.; Marcy, H. O.; Kannewurf, C. R. *J. Am. Chem. Soc.* **1989**, *111*, 4139. (c) Wu, C. G.; DeGroot, D. C.; Marcy, H. O.; Schindler, J. L.; Kannewurf, C. R.; Bakas, T.; Papaefthymiou, V.; Hirpo, W.; Yesinowski, J. P.; Liu, Y.-J.; Kanatzidis, M. G. *J. Am. Chem. Soc.* **1995**, *117*, 9229.

(4) (a) Bissessur, R.; Kanatzidis, M. G.; Schindler, J. L.; Kannewurf, C. R. *J. Chem. Soc., Chem. Commun.* **1993**, 1582. (b) Wang, L.; Schindler, J.; Kannewurf, C. R.; Kanatzidis, M. G. *J. Mater. Chem.* **1997**, *7*, 1277. (c) Tsai, H.-L.; Schindler, J. L.; Kannewurf, C. R.; Kanatzidis, M. G. *Chem. Mater.* **1997**, *9*, 875.

(5) Nazar, L. F.; Wu, H.; Power, W. P. *J. Mater. Chem.* **1995**, *5*, 1985.

(6) Wang, L.; Rocci-Lane, M.; Brazis, P. W.; Kannewurf, C. R.; Kim, Y.-Il.; Choy, W. L.; J.-H.; Kanatzidis, M. G. *J. Am. Chem. Soc.* **2000**, *122*, 6629.

(7) Yang, D.; Westreich, P.; Frindt, R. F. *Nanostruct. Mater. Part A* **1999**, *12*, 467.

(8) (a) Lemmon, J. P.; Wu, J.; Oriakhi, C.; Lerner, M. M. *Electrochim. Acta* **1995**, *40*, 2245. (b) Oriakhi, C. O.; Nafshun, R. L.; Lerner, M. M. *Mater. Res. Bull.* **1996**, *31*, 1513.

(9) (a) Yang D., Frindt R. F. *J. Mater. Res.* **2000**, *15*, 2408. (b) Sukpirom N., Oriakhi C. O., Lerner M. M. *Mater. Res. Bull.* **2000**, *35*, 325.

(10) Murphy, D. W.; Hull, Jr., G. W. *J. Chem. Phys.* **1975**, *62*, 973.

(11) Lerf, A.; Schöllhorn, R. *Inorg. Chem.* **1977**, *16*, 2950.

(12) (a) Nazar, L. F.; Jacobson, A. J. *J. Mater. Chem.* **1994**, *4*, 1419. (b) Jacobson, A. J. In *Comprehensive Supramolecular Chemistry*; Alberti, G., Bein, T., Eds.; Elsevier Science Ltd.: New York, 1996; Vol.7, pp 315.

pared H_xTaS_2 could be dispersed in aqueous surfactant solutions and form adsorption complexes with cationic dyes.[10] Later, chemically prepared Na_xTaS_2 was dispersed in water or NMF/water mixtures, and cluster cations were included to form ordered intercalation compounds.[12b] Cation intercalation is driven more or less by cation exchange and does not require an exfoliated solid.[13] Neutral polymer intercalation, however, needs a different driving force, for example, polymer$-Li^+$ interactions, van der Waals polymer$-TaS_2$ interaction, and direct coordination. The intercalation of polymers most probably takes advantage of the affinity of the macromolecular chains for the interlayer surface of the host and for the cations (i.e. Li^+) in the interlayer galleries.

Here we describe several TaS_2/polymer nanocomposites prepared through the encapsulative precipitation method.[14,15] Namely, the encapsulation of poly(ethylene oxide) (PEO), polyethylene imine (PEI), and poly(vinylpyrrolidinone) (PVP) into TaS_2 was examined in detail and the nanocomposites were characterized by a wide variety of experimental techniques. We also investigated the behavior of Li_xTaS_2 as a function of x with respect to exfoliation and polymer intercalation. We show that the value of x is critical in the synthesis of intercalative TaS_2 complexes. The difference between PEI and other polymers and the subtleties of the exfoliation and encapsulation of exfoliated TaS_2 are discussed.

Given that some metal dichalcogenides become superconductors at low temperatures, it is intriguing to consider polymer nanocomposites containing superconducting components. Such materials would combine the superconducting properties of inorganic solids with the processable properties of polymers, giving rise to new forms of superconductors such as polymer matrix-based wires and free-standing films, thus enabling new kinds of applications. This is a major advantage, because pure metal dichalcogenides are only available in polycrystalline nonprocessable forms. We have made a first step in this direction by inserting polymers into $NbSe_2$[4c] and TaS_2 to produce lamellar inorganic/polymer superconducting solids with plasticlike characteristics. This work is an outgrowth of our studies of intercalative polymer nanocomposites of MoS_2[4a] using the exfoliation procedure.[16] Remarkably, the free-standing flexible metallic TaS_2/polymer nanocomposites display bulk superconductivity.

Experimental Section

Reagents PEO (MW 5,000,000, 100,000), PEI (MW 25,000) and PVP (MW 10,000) were purchased from Aldrich Chemical Co., Inc. After the polymers were dissolved, the polymer solutions were filtered to purify from insoluble polymer

(13) Lerf, A.; Lalik, E.; Kolodziejski, W.; Klinowski, J. *J. Phys. Chem.* **1992**, *96*, 7389.
(14) A TaS_2/PEI nanocomposite by almost the same preparation approach has been reported in ref 8.
(15) Formation of polymers in TaS_2 has been know for some time. TaS_2/poly(4-vinylpyridine) intercalates were synthesized by in situ monomer insertion and interlayer gallery polymerization: (a) Hsu, C.−H.; Labes, M. M.; Breslin, J. T.; Edmiston, D. J.; Winter, J. J.; Leupold, H. A.; Rothwarf, F. *Nature, Phys. Sci.*, **1973**, *246* (155), 122. (b) Polypeptides were intercalated into 2H-TaS_2 by direct insertion: Chapela, V. M.; Parry, G. S. *Nature* **1979**, *281*, 134.
(16) (a) Joensen, P.; Frindt, R. F.; Morrison, S. R. *Mater. Res. Bull.* **1986**, *21*, 457. (b) Gee, M. A.; Frindt, R. F.; Joensen, P.; Morrison, S. R. *Mater. Res. Bull.* **1986**, *21*, 543.
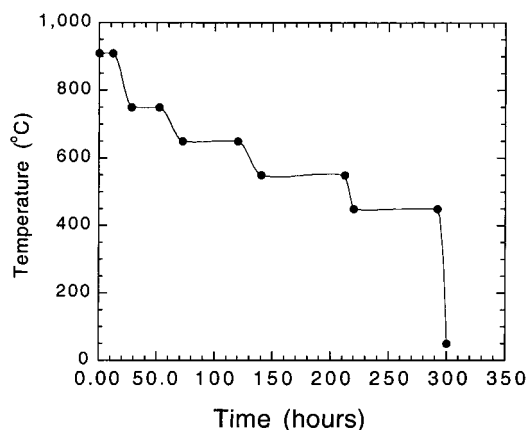

Figure 1. Annealing temperature profile of a 1T-TaS_2 sample for complete conversion to 2H-TaS_2.

residues. $LiBH_4$ (95%), $LiOH \cdot H_2O$ (98%), and Ta (99.9%, 325 mesh) were also purchased from Aldrich. Sublimed sulfur was from Spectrum Chemical Mfg. Co. Anhydrous ether (99.0%), acetonitrile (99.5%), 2-propanol (99.9%), and carbon disulfide (100%) were from Columbus Chemical Industries Inc., EM Science Inc., Mallinckrodt Chemical Inc., and J. T. Baker Inc., respectively. No further purification was applied to the chemicals above. The water was deionized and degassed by bubbling nitrogen through it for 30 min before use.

Synthesis of 2H-TaS_2. 2H-TaS_2 was synthesized according to a modified literature procedure.[17] A 3.619 g sample of tantalum (20 mmol) and 1.300 g of sulfur (40.5 mmol), sealed in a quartz tube, were heated at 450 °C for 12 h and then 950 °C for 36 h. The quartz tube was 13 mm in diameter and ∼13 cm long with a volume of about 12−14 mL. The tube was quenched from 950 °C in cold water, and excess sulfur was deposited on the tube walls. The 1T-TaS_2 formed was ground and washed with CS_2 to remove any excess sulfur. The purified 1T-TaS_2 was transformed to 2H-TaS_2 by a complex annealing procedure of slow cooling from 910 to 450 °C in 2 weeks, according to the protocol shown in Figure 1.

Synthesis and Exfoliation of Li_xTaS_2. A 4.00 g sample of 2H-TaS_2 was reacted with n equiv of $LiBH_4$ (n = 0.1, 0.2, 0.3, 0.4, 0.5, and 1.0) in 100 mL of anhydrous ether for 3 days under a nitrogen atmosphere to obtain Li_xTaS_2. Li_xTaS_2 was black when n = 0.1, 0.2 and 0.3, while it was reddish brown when $n \geq 0.4$.

Li_xTaS_2 was exfoliated in degassed water, in a concentration of 1.0 g/L, by 30 min of ultrasonic treatment under a nitrogen atmosphere. When n = 0.1, very little Li_xTaS_2 was exfoliated in water. The suspension was slightly yellowish black. When n = 0.2 or 0.3, most of the Li_xTaS_2 went into water. Especially in the case of n = 0.2, the amount of unexfoliated Li_xTaS_2 remaining was very small (∼2.6wt %) and the colloidal suspension had an intense greenish yellow color. When $n \geq$ 0.4, the Li_xTaS_2 became increasingly difficult to exfoliate. The color of the resulting suspension ranged from brownish yellow to reddish brown: the higher the value of n, the lighter the color of the suspension. Therefore, Li_xTaS_2 obtained with n = 0.2 was chosen as the host material for polymer intercalation. We will refer to this material as $Li_{0.2}TaS_2$.[18]

Encapsulative Precipitation of Polymers (Batch I and Batch II Nanocomposites). In a typical reaction, 0.40 g of $Li_{0.2}TaS_2$ was exfoliated in 400 mL of degassed H_2O by 30 min of sonication. The resulting suspension was mixed with 100

(17) Lomax, J. F. Ph.D. Dissertation, Department of Chemistry, Northwestern University, 1986.
(18) The number of equivalents, n, of $LiBH_4$ used in the lithiation reaction directly affects the value x, in Li_xTaS_2. When n is small (<0.5), x, the amount of Li in Li_xTaS_2, is expected to be close to the value of n. However, this expectation was not checked with elemental analysis. Therefore, for convenience, the nominal "$Li_{0.2}TaS_2$" is used to present the form of Li_xTaS_2 prepared under the stoichiometry n = 0.2.

mL of polymer solution (5 or 10 times in excess by equivalents of repeat units) and stirred for 2 days under a nitrogen atmosphere. The reaction mixture was then centrifuged, and almost half of the polymer/TaS₂ nanocomposite was obtained in this way and is referred to as batch I nanocomposite. After batch I was removed, the supernatant was pumped to remove most of the water. A corresponding solvent (acetonitrile for PEO and 2-propanol for PVP and PEI) was added to the concentrated supernatant to precipitate a product, which we refer to as batch II nanocomposite. The particle dimensions of TaS₂ in batch II were considerably smaller than those in batch I. The two products were pumped to dryness and vacuum-sealed in glass ampules.

Instrumentation and Measurements. Powder X-ray diffraction (XRD) patterns were obtained on a Rigaku Ru-200B X-ray diffractometer, at 45 kV and 100 mA with a scintillation counter detector and a graphite monochromator to produce Cu Kα beam (wavelength 1.54184 Å). Powder samples and a continuous scanning mode with a scanning speed of 1°/min in 2θ and an increment of 0.01° were chosen for general purpose spectra. For one-dimensional electron density calculations, we obtained XRD data (in the region $2° \leq 2\theta \leq 135°$) from highly oriented samples and a stepwise scanning mode with 0.1° per step.

Room-temperature conductivity measurements were done on pressed sample pellets with a four-probe detector connected to a Keithley-236 source-measure unit. Electrical conductivity and thermopower data were obtained with the computer-automated system described elsewhere.[19] Magnetic susceptibility measurements were done with a Quantum Design MPMS₂ SQUID magnetometer. Samples were sealed in low-density polyethylene (LDPE) bags under a nitrogen atmosphere. The magnetic contribution of the bags was measured and subtracted. Variable temperature solid state ⁷Li NMR spectra were taken on a 400 MHz Varian Instrument. Samples were loaded in a glovebox under a nitrogen atmosphere to avoid uncontrolled hydration.

Scanning electron microscopy (SEM) and energy dispersive spectroscopy (EDS) were done with a JEOL-JSM 35 CF microscope at an accelerating voltage of 15 and 20 kV, respectively. Samples were mounted on the sample stub with conductive tape. Electron diffraction was done on a transmission electron microscope (TEM) JEOL-100CX at 120 kV. Samples were ground and suspended in water or acetone before deposition on copper grids. Gold film deposited on a copper grid was used as a standard for the calibration of the camera length.

Composition of Nanocomposites. In thermogravimetric analysis (TGA) experiments under either oxygen or nitrogen flow, the nanocomposites lost very little weight up to ~190 °C (<0.5% for batch I nanocomposites and < 2.5% for batch II nanocomposites), suggesting that they contain very little water. The major weight loss step for all nanocomposites occurred between 200 °C and 350 °C and corresponds to polymer combustive decomposition. For comparison, the weight loss of Li₀.₂TaS₂ in oxygen flow was checked by TGA up to 800 °C and found to average ~8.2%. The amount of polymer in the nanocomposites was calculated by assuming that the Li₀.₂-TaS₂ in the nanocomposites also lost ~8.2% of its weight. The final product from the TGA in an oxygen flow was mainly Ta₂O₅ and a minute amount of Li₂SO₄, which was confirmed by XRD and IR spectroscopy[20]

Differential scanning calorimetry (DSC) was carried out on a Shimadzu DSC-50 under nitrogen flow of a rate of 20 mL/min. The heating and cooling rates were 5 °C/min. Sample cells made of aluminum were annealed at 450 °C in vacuum-sealed tubes after they were cleaned. Samples were sealed in cells under a nitrogen atmosphere before measurement.

One-Dimensional Electron Density Maps. One-dimensional electron density (1-D ED) maps were calculated using XRD data collected from highly oriented film samples in a stepwise scanning mode. These films were made by casting aqueous nanocomposite colloidal solutions on flat glass plates under nitrogen, so that the basal planes of the TaS₂ layers restacked parallel to the substrate. Several layers of a film were loaded in the sample plate to obtain maximum scattering intensity. The XRD experiments were carried out under a nitrogen atmosphere to avoid possible changes in the interplanar distances due to ambient moisture fluctuations. To collect the data, slits for different beam width as well as different counting times were used for different 2θ ranges, to achieve a compromise between peak broadening, peak intensity, and experiment time. Specifically, 0.5° slits and a data counting time of 3 s per step were used for $2° < 2\theta < 40°$, 1.0° slits and 3 s per step for $26° < 2\theta < 70°$, 2.0° slits and 60 s per step for $59° < 2\theta < 120°$, and 4.0° slits and 60 s per step from 101° to 135°. The step width was kept constant (0.1°) in the entire 2θ range.

A full range XRD pattern ($2° \leq 2\theta \leq 135°$) was obtained by merging the data from the different 2θ ranges and normalizing (scaling) them on the basis of the overlapped regions. The overlapped data regions had at least two peaks in common. The full data set was put into an XRD analysis program, PEAKOC,[21] to calculate the integrated peak area of each 00*l* reflection. In pattern analysis, 00*l* peaks were fit with the split-pseudo-Voigt function with a linear background subtraction for each peak. In the case that an 00*l* peak overlapped partially with another peak, or was cut off at the end of the pattern, it was fit with the pseudo-Voigt function that is symmetric.

The integrated peak area of the 00*l* peaks was used as the intensity of the peaks and put in a locally written FORTRAN program to compute the 1-D ED map as described elsewhere.[6]

Results and Discussion

Exfoliation Properties of Li$_x$TaS₂. Na$_x$TaS₂, as reported previously, did not form ideal suspensions in water, so formamide (FM), *N*-methylformamide (NMF), or NMF/H₂O 1:1 mixture were used to produce concentrated suspensions.[11,12b] FM and NMF are not preferred for the intercalation of polymers because not only are they expensive and toxic, they also compete with the polymers and cointercalate in the host. To be able to use TaS₂ as a polymer host we needed a material that exfoliated well in water. Therefore, we explored the swelling and exfoliation properties of Li$_x$TaS₂ as a function of x. Material with different degrees of lithiation was prepared with different methods: (a) reaction with butyllithium in hexane, (b) reaction with Na₂S₂O₄ in water followed by ion-exchange with Li⁺ ions, and (c) reaction with LiBH₄ in ether and in various stoichiometric ratios and conditions. The LiBH₄ method [22] was most successful and the best Li$_x$TaS₂ suspension was obtained with $x \sim 0.2$. Namely, Li₀.₂TaS₂ formed concentrated and stable single layer colloidal solutions in water, superior to those formed with Na$_x$TaS₂ in NMF/H₂O solution.

Usually, the more readily Li$_x$TaS₂ exfoliates the more concentrated suspension it forms and the less residue it leaves behind. Nevertheless, in all cases, there was always a fraction of Li$_x$TaS₂ that did not exfoliate, regardless of how dilute the solution was.

To demonstrate how the amount of LiBH₄ affected the exfoliation of Li$_x$TaS₂, a quantitative experiment was

(19) Lyding, J. W.; Marcy, H. O.; Marks, T. J.; Kannewurf, C. R. *IEEE Trans. Instrum. Meas.* **1988**, *37*, 76.

(20) For Li₀.₂TaS₂ to become Li₂SO₄ and Ta₂O₅, the weight loss should be 5.9%. Because Li compounds can be volatile at high temperatures, the weight loss of the sample in oxygen flow could be somewhat higher than the theoretical value.

(21) PEAKOC is an XRD powder pattern analysis program provided by Inel Inc. (Mail Address in U.S.A.: P.O. Box 147, Stratham, NH 03885.)

(22) Kanatzidis, M. G.; Marks, T. J. *Inorg. Chem.* **1987**, *26*, 783.

Table 1. Polymer Intercalation in Li_xTaS_2 as a Function of Degree of Lithiation

	intercalation of polymers[a]		
n	PEI	PVP	PEO
0.1	yes	no	
0.2	yes	yes	yes
0.3	yes	yes	
0.4	yes	yes	no
0.5	yes	no	
1.0	yes		no

[a] "Yes" indicates that the intercalation was successful, while "no" shows that it failed.

performed with 0.050 g of Li_xTaS_2 with $n = 0.1, 0.2, 0.3$, and 0.4. After Li_xTaS_2 was sonicated for 30 min in 200 mL of degassed water, the remaining solids were collected, dried, and weighed. On the basis of the Li_xTaS_2 used, the unexfoliated fraction was 53%, 2.6%, 21%, and 21%, respectively, for $n = 0.1, 0.2, 0.3$, and 0.4. These results showed that 0.1 equiv of $LiBH_4$ was not adequate, while 0.3 or 0.4 equiv of $LiBH_4$ was over the optimum ratio. It needs to be pointed out that the charge density of $Li_{0.2}TaS_2$, ~ 48 $Å^2/e^-$, is close to the upper limit of the $40-120$ $Å^2/e^-$ range[23] in which stable colloidal dispersions are most likely to form.

Li_xTaS_2 used by Oriakhi et al.[8] to prepare the PEI/TaS_2 nanocomposite was lithiated by reacting with $LiOH$.[24] Our investigation into this type of lithiation revealed that control of the $LiOH$ concentration is equally important and the optimum stoichiometric ratio is approximately the same as for $LiBH_4$.

Nanocomposites by Polymer Encapsulation. The success of polymer encapsulation depends on the nature of both Li_xTaS_2 and polymer. Table 1 shows which attempts succeeded in the preparation of nanocomposites. PEO was intercalated only in "$Li_{0.2}TaS_2$". PVP was intercalated in Li_xTaS_2 prepared with $0.2 < x < 0.4$. PEI has the greatest affinity and intercalated in all Li_xTaS_2 samples.[25] This must be due to the fact that PEI is a strong organic base that could be protonated in solution. The protonated form has positive charge that facilitates the interaction with the $[TaS_2]^{x-}$ layers. In this sense, the insertion of PEI in $[TaS_2]^{x-}$ is an ion-exchange process where Li^+ ions are replaced with positively charged PEI molecules. Other polymers such as polyacrylamide (PAM) and methyl cellulose (MCel) were also tried. Partial intercalation was achieved with PAM but not with MCel.

Characterization of Li_xTaS_2/Polymer Nanocomposites. The formation of lamellar Li_xTaS_2/polymer nanocomposites was evident in the XRD patterns of the products. The presence and position of $00l$ reflections indicated the separation of the TaS_2 slabs, which is evidence for the insertion of polymer chains. The pristine TaS_2 and the hydrated $Li_x(H_2O)_yTaS_2$ ($x \sim 0.2$) show interlayer spacings of 6.0 and 7.4 Å, respectively, which can be readily distinguished from a polymer intercalated phase. The d spacings of batches I and II for both PEO and PVP nanocomposites were comparable
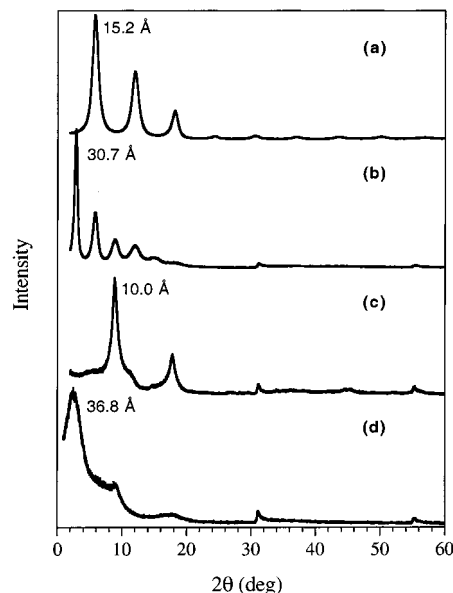
(23) Jacobson, A. *Mater. Sci. Forum* **1994**, *1*, 152.
(24) Biberacher, W.; Lerf, A.; Buheitel, F.; Butz, T.; Hübler, A. *Mater. Res. Bull.* **1982**, *17*, 633.
(25) PEI was also intercalated in heavily lithiated Li_xTaS_2 prepared from either $2H\text{-}TaS_2$ or $1T\text{-}TaS_2$ through a solid-state reaction with 3 equiv of $LiBH_4$ in the temperature range from 300 to 525 °C.

Figure 2. XRD patterns of Li_xTaS_2/polymer nanocomposites with Cu Kα radiation: (a) $Li_{0.2}(PEO)_yTaS_2$ (batch II), (b) $Li_{0.2}(PVP)_yTaS_2$ (batch II), (c) $Li_x(PEI)_yTaS_2$ (batch I), and (d) $Li_x(PEI)_yTaS_2$ (batch II).

within ± 1 Å. The XRD patterns of the two types of products were similar, except that in batch I we could observe weak diffraction lines from residual unintercalated solid. In the case of PEI, the d spacing of batch I product was about 10.0 Å, while that of batch II product was about 37 Å, indicating the encapsulation of multiple layers of polymer. Some typical XRD patterns of the nanocomposites are shown in Figure 2.

More information about d spacings and coherence lengths perpendicular to the layers is listed in Table 2. From these data, one can estimate the ordered domains in particles of the nanocomposites to be between 5 and 10 TaS_2 layers thick. $Li_x(PEI)_y(H_2O)_zTaS_2$ (batch I) has the largest number of coherent layers, ~ 9; $Li_{0.2}(PVP)_y(H_2O)_zTaS_2$ has $\sim 6-8$; and $Li_{0.2}(PEO)_y(H_2O)_zTaS_2 \sim 5-7$. Table 2 also lists the compositions of the nanocomposites. It is obvious that a batch II nanocomposite contains a little more polymer than its batch I analogue. This is understandable because batch II product was well-dispersed in water due to smaller TaS_2 particles and interacted more extensively with the dissolved polymer.

DSC measurements on $Li_{0.2}(PEO)_{1.04}TaS_2$ samples showed no phase transition between room temperature and 300 °C (see Figure 3). The melting peak of PEO at 66 °C is not observed in the nanocomposite. A small exothermic peak at 308 °C (2.21 J/g) and a large one at 330 °C (46.18 J/g) correspond to the decomposition of PEO and are associated with massive weight loss detected by TGA. Pure PEO shows an exothermic decomposition peak around 370 °C.

The pyrolysis mass spectra of the $Li_{0.2}(PEO)_{1.04}TaS_2$ samples in a rising temperature ramp showed that the major decomposition fragments at ~ 350 °C had molecular masses of 45, 58, 73, 87, 88, 89, 103, 120, 133, and so on, which were all PEO related fragments. There was no obvious evidence that these decomposition fragments combined with sulfur from the TaS_2 layers. [26]

The Li_xTaS_2/polymer nanocomposites, described here, can be cast into free-standing films. The films of batch

Table 2. Properties of Li$_{0.2}$TaS$_2$ and Polymer Nanocomposites

sample	d spacing (Å)	coherence length^a (Å)	composition	room temperature conductivity (S/cm)
Li$_{0.2}$TaS$_2$	6.0			>10^3
hydrated Li$_{0.2}$TaS$_2$	7.4			
Li$_{0.2}$(PEO)$_y$TaS$_2$ (batch I)	15.6	93	Li$_{0.2}$(PEO)$_{1.36}$TaS$_2$	19
Li$_{0.2}$(PEO)$_y$TaS$_2$ (batch II)	15.2	83	Li$_{0.2}$(PEO)$_{1.51}$(H$_2$O)$_{0.23}$TaS$_2$	2.2
Li$_{0.2}$(PEO)$_y$TaS$_2$ (batch I)	15.1	106	Li$_{0.2}$(PEO)$_{0.75}$(H$_2$O)$_{0.06}$TaS$_2$	17
Li$_{0.2}$(PEO)$_y$TaS$_2$ (batch II)	15.5	83	Li$_{0.2}$(PEO)$_{1.68}$TaS$_2$	3.0
Li$_{0.2}$(PVP)$_y$TaS$_2$ (batch I)	31.1	256	Li$_{0.2}$(PVP)$_{0.95}$TaS$_2$	31
Li$_{0.2}$(PVP)$_y$TaS$_2$ (batch II)	30.7	186	Li$_{0.2}$(PVP)$_{1.28}$(H$_2$O)$_{0.35}$TaS$_2$	0.5
Li$_{0.2}$(PEI)$_y$TaS$_2$ (batch I)	10.0	93	Li$_x$(PEI)$_{0.82}$TaS$_2$	125
Li$_{0.2}$(PEI)$_y$TaS$_2$ (batch II)	36.8	NA	Li$_x$(PEI)$_{3.2}$(H$_2$O)$_{0.56}$TaS$_2$	0.18

^{a} X-ray scattering coherence lengths were calculated from the Scherrer formula $L_{hkl} = K\lambda/\beta \cos \theta$ ($K \sim 0.9$). (Klug, H. P.; Alexander, L. E. *X-ray Diffraction Procedures for Polycrystalline and Amorphous Materials*, John Wiley & Sons, New York, 1962, pp 491.
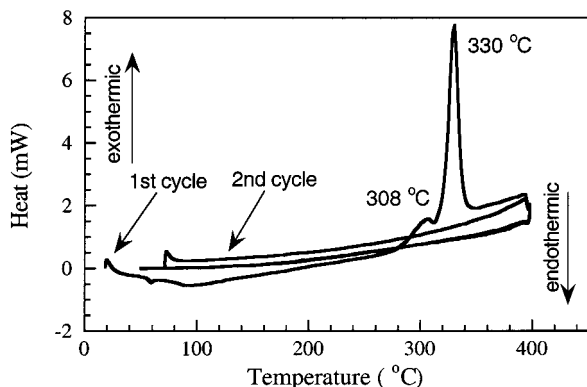
Figure 3. DSC scan of a sample of Li$_{0.2}$(PEO)$_{1.04}$TaS$_2$.

II are stronger than those of batch I and can be folded without breaking. This is attributed to the higher polymer content of the batch II materials. Figure 4 shows an SEM photo of a folded Li$_{0.2}$(PEO)$_{1.68}$TaS$_2$ film (batch II, MW = 5 000 000). The film was folded before it was pressed onto the conductive tape. The folding edge did not crack under pressure.

Structural Studies: The Conformation of PEO in Li$_x$(PEO)$_y$TaS$_2$. The conformation and orientation of polymer chains in the interlayer galleries of the layered nanocomposites have always been important issues. There are many known PEO chain conformations. The most common is the helical conformation,[27] which exists in PEO spherulites.[28] Planar zigzag conformation was obtained in stretched PEO samples,[29] and two kinds of conformations were found in PEO−HgCl$_2$ complexes.[30,31] Additional PEO conformations have been found in other complexes in the literature.[32] Models for the most important PEO conformations are shown in

Figure 4. SEM photograph of a folded Li$_{0.2}$(PEO)$_{1.68}$TaS$_2$ film. The sample is ∼2 cm long.

Figure 5. In previous work we calculated 1-D ED maps for (PEO)$_x$V$_2$O$_5$·nH$_2$O[33] and determined that the helical conformation of PEO in that nanocomposite was not possible. A bilayer planar zigzag structure was proposed.

In the present case, films of batch II Li$_{0.2}$(PEO)$_y$TaS$_2$ nanocomposite had well-defined sharp XRD patterns with 17 00l reflections corresponding to a resolution of 0.85 Å (see Figure 6). This intense XRD pattern offered a good starting point for 1-D ED calculation for Li$_{0.2}$(PEO)$_y$TaS$_2$ and provided useful information on the internal structure of the intercalated species projected on the c-axis. As mentioned in the Experimental Section, the phases for calculating this 1-D ED map were obtained from the positions of the Ta and S atoms, which are taken to be known.

(26) The Li$_{0.2}$TaS$_2$ and Li$_{0.2}$(PEO)$_{1.04}$TaS$_2$ were heated to 350 °C under nitrogen atmosphere and kept for 10 min at this temperature to check if there was any loss of sulfur from the TaS$_2$ layers. The sulfur content in these two samples as well as the untreated samples was checked with EDS, using 2H-TaS$_2$ as a standard. The stoichiometric number for sulfur, m (as TaS$_m$), was in the range $1.96 < m < 2.01$. This indicates that almost no sulfur is lost in the lithiation, intercalation, or heating treatment of Li$_{0.2}$TaS$_2$ and Li$_{0.2}$(PEO)$_{1.04}$TaS$_2$ up to 350 °C under nitrogen. This is consistent with TGA, which showed that Li$_{0.2}$TaS$_2$ had no weight loss in nitrogen up to 530 °C.

(27) (a) Takahashi, Y.; Tadokoro, H. *Macromolecules* **1973**, *6*, 672. (b) Brandrup, J.; Immergut, E. H. *Polymer Handbook*, 3rd ed.; John Wiley & Sons: New York, 1989, pp VI/72.

(28) Price, F. P.; Kilb, R. W. *J. Polym. Sci.* **1962**, *57*, 395.

(29) Takahashi, Y.; Sumita, I.; Tadokoro, H. *J. Polym. Sci., Polym. Phys. Ed.* **1973**, *11*, 2113.

(30) Iwamoto, R.; Saito, Y.; Ishihara, H.; Tadokoro, H. *J. Polym. Sci., A-2*, **1968**, *6*, 1509.

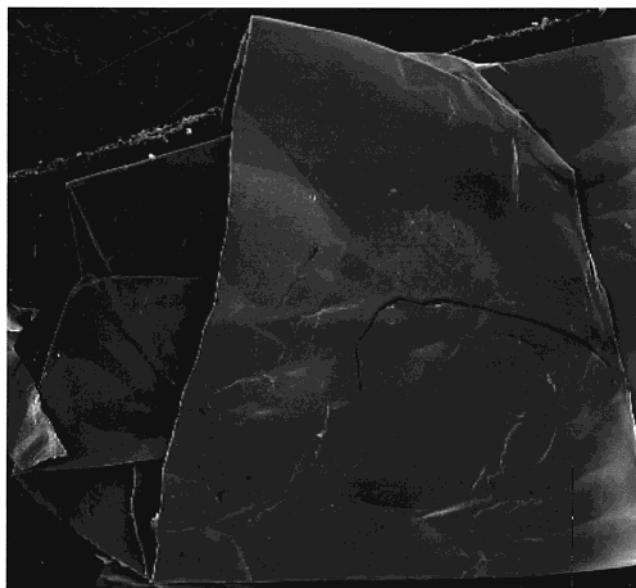(31) Yokoyama, M.; Ishihara, H.; Iwamoto, R.; Tadokoro, H. *Macromolecules* **1969**, *2*, 184.

(32) (a) Chatani, Y.; Okamura, S. *Polymer* **1987**, *28*, 1815. (b) Lightfoot, P.; Mehta, M. A.; Bruce, P. G. *Science* **1993**, *262*, 883. (c) Lightfoot, P.; Nowinski, J. L.; Bruce, P. G. *J. Am. Chem. Soc.* **1994**, *116*, 7469. (d) Lightfoot, P.; Mehta, M. A.; Bruce, P. G. *J. Mater. Chem.* **1992**, *2*, 379. (e) Chatani, Y.; Fujii, Y.; Takayanagi, T.; Honma, A. *Polymer* **1990**, *31*, 2238. (f) Tadokoro, H.; Yoshihara, T.; Chatani, Y.; Murahashi, S. *J. Polym. Sci. B.* **1964**, *2*, 363. (g) Tadokoro, H. *Macromol. Rev.* **1966**, *1*, 119. (h) Point, J. J.; Coutelier, C. *J. Polym. Sci., Polym. Phys. Ed.* **1985**, *23*, 231. (i) Point, J. J.; Damman, P. *Macromolecules* **1992**, *25*, 1184. (j) Damman, P.; Point, J. J. *Macromolecules* **1994**, *27*, 3919.

(33) Liu, Y.-J.; Schindler, J. L.; DeGroot, D. C.; Kannewurf, C. R.; Hirpo, W.; Kanatzidis, M. G. *Chem. Mater.* **1996**, *8*, 525.
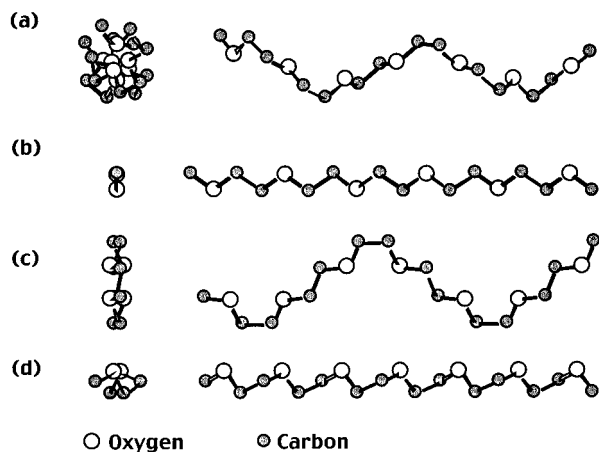
Figure 5. Possible PEO conformations: (a) helical, (b) planar zigzag, (c) conformation in PEO−HgCl$_2$ complex (type I), and (d) conformation in PEO−HgCl$_2$ complex (type II).
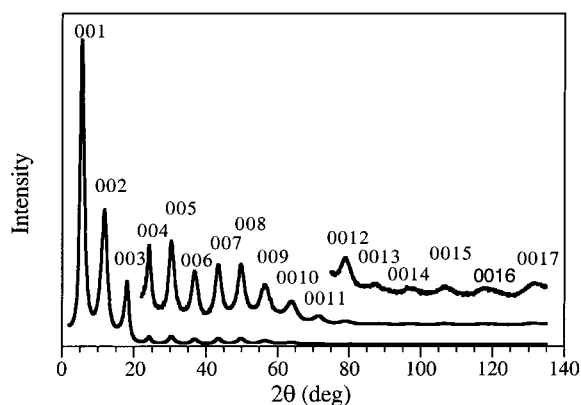

Figure 6. XRD pattern of an oriented Li$_{0.2}$(PEO)$_y$TaS$_2$ film sample (batch II; MW ∼ 100 000) with Cu Kα radiation.

Figure 7. One-dimensional electron density maps projected on the *c*-axis for the Li$_x$(PEO)$_y$TaS$_2$ nanocomposite. The Ta atoms are at $x = 0$ and 1. The sulfur atom positions are indicated. (a) Model with two layers of planar zigzag PEO chains with the planes perpendicular to the TaS$_2$ layers. (b) Model with two layers of planar zigzag PEO chains with the zigzag planes parallel to the TaS$_2$ layers. (c) Model with two layers of PEO in the type II PEO−HgCl$_2$ complex conformation and (d) derived from experimental diffraction data.

The 1-D ED map for Li$_{0.2}$(PEO)$_y$TaS$_2$ clearly shows the presence of substantial electron density between the TaS$_2$ slabs (see Figure 7d). This density is due to the organic polymer and it is distributed away from the center of the gallery, peaking in two separate locations symmetrically above and below the gallery central plane. The peak shape in each location is asymmetric. This immediately excludes the helical conformation of PEO, which must have one symmetric broad envelope of electron density in the central region of the gallery. The observed profile in Li$_{0.2}$(PEO)$_y$TaS$_2$ is also different from that of the (PEO)$_x$V$_2$O$_5$·nH$_2$O system, which displays two symmetric bumps with two maxima on each of them, so the planar zigzag model does not fit here. Parts a and b of Figure 7 present the profiles of the 1-D ED map calculated for two layers of planar zigzag PEO chains arranged parallel and perpendicular inside the gallery space of TaS$_2$.[34] As expected, they have two symmetric bumps and their maxima are too far apart to match the profile calculated from XRD data of Li$_{0.2}$(PEO)$_y$TaS$_2$.

The structural model best matching the experimental data is set up with two layers of PEO with the
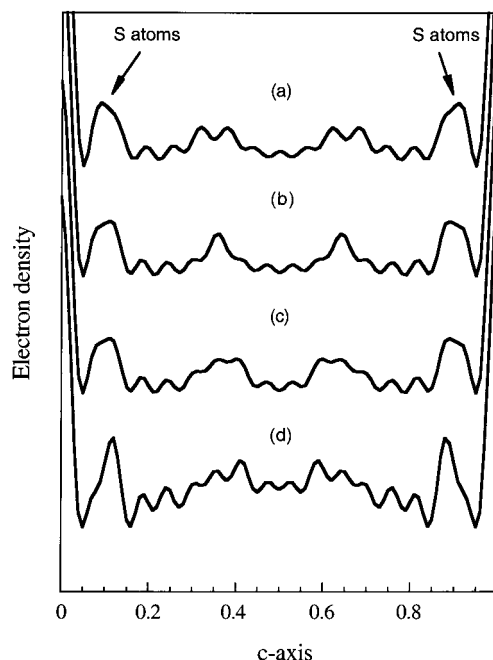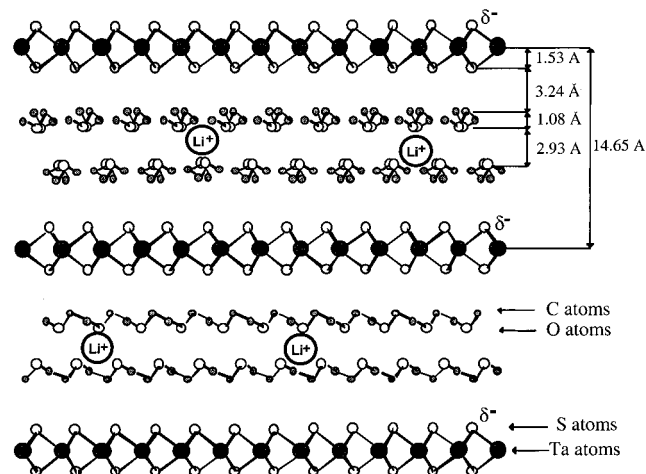

Figure 8. Structural model for the Li$_{0.2}$(PEO)$_y$TaS$_2$ nanocomposite. The oxygen atom region in the middle of the gallery accommodates the Li$^+$ ions. The distances shown indicate the corresponding spacings in projection.

conformation found in the type II PEO−HgCl$_2$ complex. This conformation has oxygen atoms on one side and carbon and hydrogen atoms on the other side of the molecule. By placing two layers of PEO inside the gallery, so that the oxygen atoms face each other in the middle of the gallery, as shown in the model in Figure 8, two asymmetric bumps appear in the electron density map. The positions of the atoms can be estimated by fitting maxima of the bumps (see Figure 7c). In this model, the atoms of PEO occupy reasonable positions in the gallery. In addition, the orientation of the PEO chains is chemically plausible because the hydrophobic

(34) The positions of the atoms of PEO of were estimated from the structural data available from the crystal structure with planar zigzag conformation (ref 29). When the ac plane of the unit cell is parallel to the layers, the PEO zigzag plane is almost parallel to the TaS$_2$ layers; when the bc plane of the unit cell is parallel to the TaS$_2$ layers, the PEO zigzag plane is almost perpendicular to the layers.

Table 3. Superconducting Properties of the Polymer/TaS₂ Intercalates[a]

sample	sample state	T_c (K)	χ_{molar} (2 K, 5 G)	% pure superconductor
Li$_x$TaS$_2$ ($n = 0.2$)	powder	3.7, 4.3	-2.64	82
Li$_x$TaS$_2$ ($n = 0.4$)	powder	4.1, 4.6	-0.128	4.0
Li$_x$TaS$_2$ ($n = 0.5$)	powder	2.7, 4.3	-1.1×10^{-3}	3.4×10^{-2}
Li$_x$(PEI)$_y$TaS$_2$ (batch I)	powder	2.9	-0.60	14
Li$_{0.2}$(PVP)$_y$TaS$_2$ (batch I)	powder	2.5	-0.82	5.8
Li$_{0.2}$(PEO)$_y$TaS$_2$ (batch I)	film parallel	2.7	-0.17	
	film perpendicular	2.6	-2.7	42
Li$_{0.2}$(PEO)$_y$TaS$_2$ (batch II)	film parallel	2.9	-5.6×10^{-3}	
	film perpendicular	2.9	-5.8×10^{-2}	0.9

[a] Densities of the materials are needed in the calculation. The density of 2H-TaS$_2$, 6.075 g/cm³, is used in the calculation of Li$_x$TaS$_2$ (n = 0.2, 0.4, and 0.5). The densities deduced from the compositions and structural parameters of the nanocomposites are used in the calculation of the superconducting fractions in the nanocomposites.

part of the PEO ($-CH_2CH_2-$ groups) forms van der Waals contacts with the sulfur atoms in the TaS$_2$ layers. On the other hand, the oxygen atoms form a more polar, hydrophilic environment in which, presumably, the small Li$^+$ cations reside. This model not only matches the experimental data, it also makes good chemical sense. The type II PEO$-$HgCl$_2$ complex conformation proposed here is probably brought about by coordinating interactions of PEO with the Li$^+$ ions, just as for the HgCl$_2$ complex. That the PEO conformation in Li$_x$(PEO)$_y$TaS$_2$ is different from that of (PEO)$_x$V$_2$O$_5 \cdot n$H$_2$O[33] is attributed to the lack of coordinating ions (e.g. Li$^+$) in the latter.

This type II structure is similar to that of the Li$_x$(PEO)$_y$RuCl$_3$ nanocomposite,[6] in which a similar electron density map along the stacking c-axis also suggested a structural model that fills each gallery with two layers of polymer chains in the conformation found in type II PEO$-$HgCl$_2$.

Superconducting State. The magnetic properties of Li$_x$TaS$_2$ and nanocomposites were measured with a SQUID. As observed earlier with the NbSe$_2$ system,[4c] the lamellar nanocomposites reported here undergo superconducting transitions at temperatures higher than that of the pristine 2H-TaS$_2$, 0.6 K (or 0.8 K according to different publications). It is known that the T_c of TaS$_2$ is pushed down by the periodic lattice distortion$-$charge density wave (PLD$-$CDW) of TaS$_2$. If the PLD$-$CDW is suppressed, the T_c could be raised to 4.1$-$4.5 K. In fact, 0.08 equiv of electrons are enough to suppress the PLD$-$CDW in TaS$_2$.[34–36] Therefore, in the Li$_x$TaS$_2$ we expect a higher T_c. The Cooper pairs in the superconducting state have a coherence length in the magnitude of a micron. This spatial correlation length is much longer than the gallery space in the Li$_x$TaS$_2$/polymer nanocomposites, which is occupied by the insulating polymer chains. That the intercalation of polymers (at least up to a certain expansion of the TaS$_2$ layers) does not destroy the superconducting state raises the question of whether the Cooper pairs can penetrate the barrier of the polymer layers and move around in the nanocomposites.

Measurements of T_c and Meissner effect are summarized in Table 3. A pure superconductor has the magnetic susceptibility of $\chi = -1/4\pi$. The superconducting fraction in the samples is calculated by comparing the susceptibility of the samples at 2 K with $-1/4\pi$. The

high percentages found in many of the nanocomposites indicate that we are observing bulk superconductivity. The T_c values were determined by the point of intersection of the extrapolations from the linear magnetization of the superconducting state and the normal-state magnetization.

The Li$_x$TaS$_2$ (n = 0.2, 0.4, and 0.5) samples exhibit two T_c values, so they are mixed-phase superconductors. This can be compared to the multiphase samples prepared from reaction of 2H-TaS$_2$ with less than 0.5 equiv of NaOH reported by Biberacher et al.[24] After Li$_{0.2}$TaS$_2$ is intercalated with polymers, the second phase disappears or is not detectable, perhaps because T_c moves to lower temperature.

From Table 3, it can be seen that the more TaS$_2$ is reduced, the lower the percentage of superconducting state in the sample. From Li$_x$TaS$_2$ (n = 0.2) to Li$_x$TaS$_2$ (n = 0.5), the value decreases 3 orders of magnitude, demonstrating the enormous effect of added electrons to the electronic structure. The intercalation of polymers causes the superconducting fraction to drop, but not by orders of magnitude; see Table 3 for Li$_x$(PEI)$_y$TaS$_2$ and Li$_{0.2}$(PVP)$_y$TaS$_2$ and the film sample of batch I Li$_{0.2}$(PEO)$_y$TaS$_2$. The small superconducting fraction of batch II Li$_{0.2}$(PEO)$_y$TaS$_2$ films could be due to the smaller size of the TaS$_2$ slab particles in the nanocomposite.

Field dependent magnetic measurements on Li$_x$TaS$_2$ and the nanocomposites show that the Meissner effect decreases with increasing magnetic field. Variable temperature magnetic susceptibility measurements show that the Meissner effect decreases gradually with increasing temperature. Furthermore, the field cooling curve diverges from the zero-field cooling curve in these materials, which is consistent with a type II superconductor.[37]

In variable temperature magnetic susceptibility measurements, the field cooling curve was very different from the zero-field cooling curve for Li$_{0.2}$TaS$_2$ (Figure 9a), while the two curves were much closer together in batch I Li$_{0.2}$(PEO)$_y$TaS$_2$ (Figure 9b). The two curves of batch II Li$_{0.2}$(PEO)$_y$TaS$_2$ were also close together. The drift of the field cooling curve toward the zero-field cooling curve, which was also found in the PEI and PVP intercalated nanocomposites, indicates that these materials are less able to pin the electromagnetic vortices present. This is typical of granular superconductivity,

(35) Garoche, P.; Manuel, P.; Veyssie, J. J.; Molinié, P. *J. Low. Temp. Phys.* **1978**, *30*, 323.
(36) Friend, R. H.; Yoffe, A. D. *Adv. Phys.* **1978**, *36*, 1.

(37) Kresin, V. Z.; Wolf, S. A. *Fundamentals of Superconductivity*, Plenum Press: New York/London, 1990; p 95.
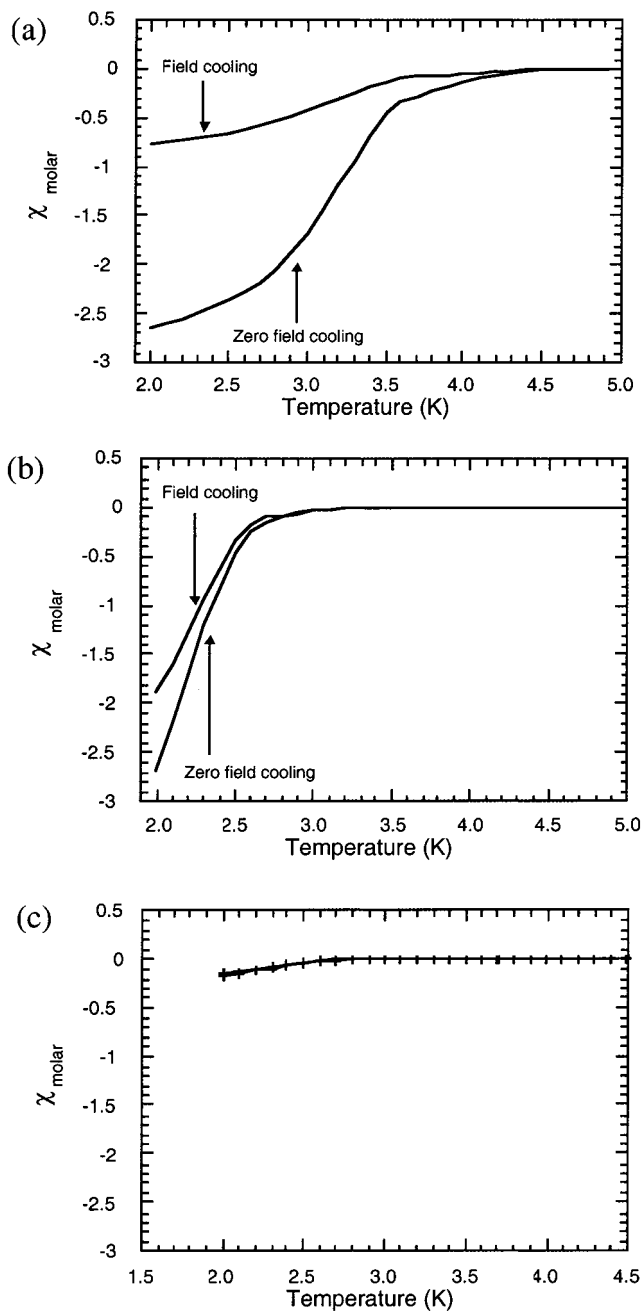
Figure 9. Variable temperature magnetic susceptibility (at 5 G) for (a) $Li_{0.2}TaS_2$ (powder) and (b) $Li_{0.2}(PEO)_yTaS_2$ (batch I; MW $\sim$ 100 000; films perpendicular to the applied magnetic field). (c) $Li_{0.2}(PEO)_yTaS_2$ films parallel to the applied magnetic field. (units of χ_{molar} are emu/mol).

which appears in materials composed of tiny grains of superconductor particles surrounded by insulating layers.[37] In contrast, $NbSe_2$ nanocomposites did not show this effect.[4c]

A dramatic difference is observed with sample orientation in the magnetization curves below T_c (see Figure 9b,c). The Meissner effect is much stronger when the film is placed perpendicular to the magnetic field. In both batches I and II Li_xTaS_2/PEO samples, the χ_{molar} was >10 times larger when the film was perpendicular to the field (i.e. TaS_2 layers perpendicular to field) than when it was parallel. This observation suggests that the Cooper pairs are moving predominantly in circular orbits within the TaS_2 layers without passing through
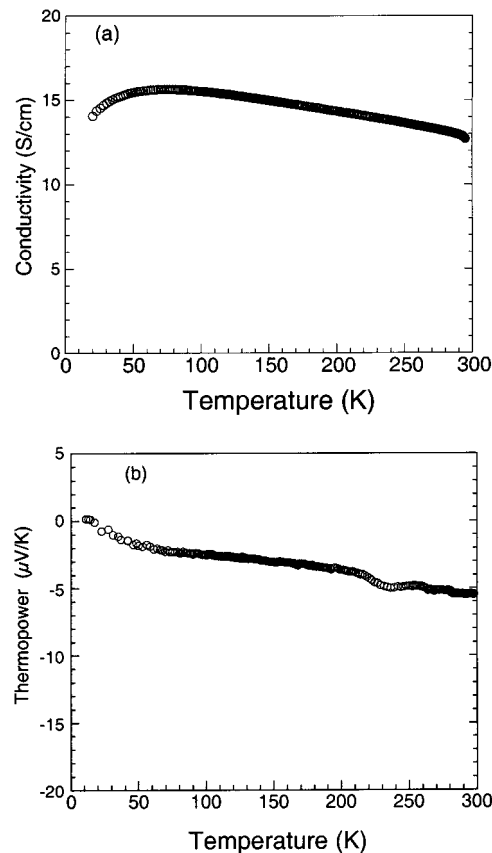

Figure 10. (a) Variable temperature electrical conductivity data and (b) thermopower data for pressed pellets of $Li_{0.2^-}$ $(PEO)_{1.04}TaS_2$ (batch I product).

the polymer layers. This is a beautiful demonstration of the two-dimensional nature of these nanocomposites.

The magnetic properties of Li_xTaS_2 and Li_xTaS_2/ polymer nanocomposites were also measured at temperatures above T_c. In this temperature range the magnetic susceptibility of Li_xTaS_2 (n = 0.2 and 0.4) was Pauli-like and temperature independent with molar χ_{TIP} around 10^{-4} cm^3/mol.

Charge Transport Properties. Room-temperature electrical conductivity measurements show that $Li_{0.2^-}$ TaS_2 and its nanocomposites are good conductors (see Table 2). $Li_{0.2}TaS_2$ itself is highly conductive, with a conductivity higher than 1000 S/cm for cold pressed pellets. The intercalation of polymers reduces the conductivity by several orders of magnitude. The batch I nanocomposites are 1–2 orders of magnitude less conductive, while the batch II products are 3–4 orders of magnitude less conductive. This is reasonable since the batch II materials contain more polymer, have greater inter-TaS_2 slab separations, and have slab particles of smaller dimensions. Variable temperature measurements for batch I and batch II of $Li_{0.2}(PEO)_y$-TaS_2 showed that the conductivity of both slightly increases with falling temperature, consistent with metallic charge transport which persists despite the granular nature of these materials (see Figure 10a). The conductivity reached a broad maximum at $\sim$75 K in batch I $Li_{0.2}(PEO)_yTaS_2$ and at $\sim$130 K in batch II $Li_{0.2}(PEO)_yTaS_2$ before it started to drop. The weak temperature dependence, and the observed conductivity values are substantially affected by the great number of grain boundaries in the samples. The superconducting

behavior was not detected, because our experimental setup could not reach the low temperature at which this transition occurs.

The metallic character is further confirmed by thermopower data shown in Figure 10b. The Seebeck coefficient is very small and negative, suggesting n-type metallic behavior. The Seebeck coefficient better represents the true charge transport behavior of the materials, since it is insensitive to grain boundaries. The n-type transport is somewhat surprising, since one might expect them to be hole conductors, given that 2H-TaS_2 has a half-filled conduction band and injection of a small amount of electrons should result in a band that is more than half-filled. The failure of this prediction could be due to the formation of a superlattice in the reduced TaS_2 layers.[38] This superlattice is believed to be due to clustering through Ta–Ta interactions within the layer that leads to a modification of the electronic band structure and of course the charge transport properties.

The above data strongly indicate that the intrinsic charge transport within the layers is metallic. However, when the carriers go through the boundary areas and polymer layers, e.g., transport perpendicular to the layers, activation energy is needed. This can contribute to a thermally activated behavior of the conductivity, especially when the TaS_2 slabs become more separated by increasing polymer content.

Solid-State NMR Spectroscopy. To probe the behavior of lithium ions in the two different gallery environments (i.e. gallery with and without polymer), we measured the variable temperature *static* solid-state ^7Li NMR spectra for $Li_{0.2}TaS_2$ and $Li_{0.2}(PEO)_yTaS_2$ (batch II). Examination of the temperature dependence of the ^7Li NMR line-width (the width at half-height) provides an independent perspective on the cation mobility in inhomogeneous solids, especially in (Li salt)/polymer complexes[39,40] and Li/polymer/inorganic nanocomposites.[41] Both $Li_{0.2}TaS_2$ and $Li_{0.2}(PEO)_yTaS_2$ showed well-defined resonance peaks due to a first-order quadrupolar transition with no significant satellite peaks.

The spectra of $Li_{0.2}TaS_2$ at −80 and 100 °C are presented in Figure 11a,b. At −80 °C, $Li_{0.2}TaS_2$ exhibits a broad peak with the maximum situated at a chemical shift of 5.5 ppm higher than the solid LiCl reference. The peak was somewhat asymmetric with a barely noticeable shoulder on the low field side. With rising temperature, the position of the peak maximum did not change, but the shoulder protruded more and moved toward lower field. At 100 °C, the shoulder became a second peak at a chemical shift of 15 ppm higher than that of LiCl. The shape and position of the peaks changed reversibly over many cooling and heating cycles. The change of the line-width of the entire peak,
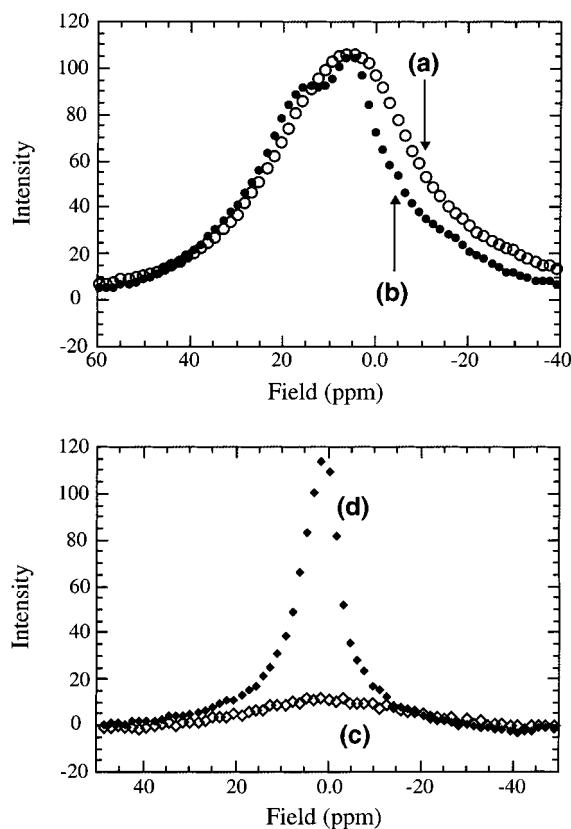
(38) Superlattice formation upon intercalation has been observed: Remskar, M.; Popovic, A.; Starnberg, H. I. *Surf. Sci.* **1999**, *430*, 199.
(39) (a) Panero, S.; Scrosati, B.; Greenbaum, S. G. *Electrochim. Acta* **1992**, *40*, 1533. (b) Gorecki, W.; Belorizky, E.; Berthier, C.; Donoso, P.; Armand, M. *Electrochim. Acta* **1992**, *37*, 1685.
(40) (a) Chung, S. H.; Jeffrey, K. R.; Stevens, J. R. *J. Chem. Phys.* **1991**, *94*, 1803. (b) Donoso, J. P.; Bonagamba, T. J.; Frare, P. L.; Mello, N. C.; Magon, C. J.; Panepucci, H. *Electrochim. Acta* **1995**, *40*, 2361.
(41) (a) Wong, S.; Vasudevan, S.; Vaia, R. A.; Giannelis, E. P.; Zax, D. B. *J. Am. Chem. Soc.* **1995**, *117*, 7568. (b) Wong, S.; Zax, D. B. *Electrochim. Acta* **1997**, *42*, 3513. (c) Yang, D.-K.; Zax, D. B. *J. Chem. Phys.* **1999**, *110*, 5325.
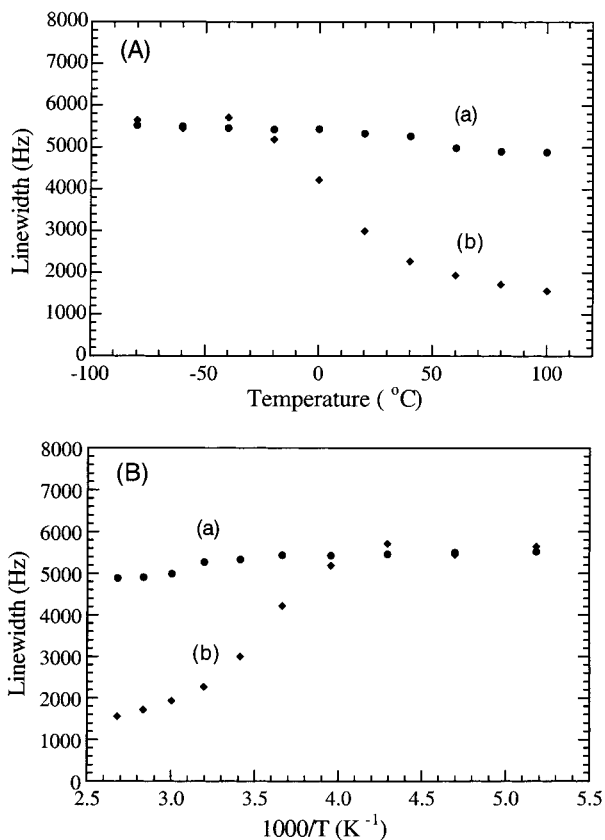

Figure 11. Static solid-state ^7Li NMR spectra of (a) $Li_{0.2}TaS_2$ at −80 °C and (b) at 100 °C and (c) $Li_{0.2}(PEO)_{1.04}TaS_2$ (batch II; MW ~ 100 000) at −80 °C and (d) at 100 °C.

versus temperature, is presented in Figure 12A(a). The broadening of the ^7Li resonance at low temperature is mostly due to many overlapping signals, corresponding to slightly different lithium ion sites. The slow decrease of the line-width with increasing temperature suggests that there is a large activation barrier for Li^+ to hop from site to site. The presence of the shoulder in the spectrum indicates a different chemical environment for Li^+ ions, which might be related to the multiphase observed in the superconducting state discussed above.

The low temperature (−80 °C) static solid-state ^7Li NMR spectra of $Li_{0.2}(PEO)_yTaS_2$ (batch II) showed a broad symmetric resonance peak with a chemical shift almost identical to that of solid LiCl (see Figure 11c). With increasing temperature, the position of the peak did not change, but its shape became sharp and slightly asymmetric (see Figure 11d). The peak base on the low field side extended a little farther than on the opposite side. The line-width did not change appreciably in the temperature range from −80 to −40 °C but it narrowed dramatically from −40 to 60 °C and then continued to narrow, albeit at a lower rate. At 100 °C, the line-width of the peak was only 28% of that at −80 °C (see Figure 12A(b)).

This temperature behavior has been attributed to dynamical motional narrowing and has been studied in many solid polymer electrolytes,[40,41] as well as PEO and poly(ethylene glycol) (PEG) nanocomposites.[41] The change in line-width is caused by the averaging of magnetic couplings over the local magnetic field associated with other neighboring spins such as other Li nuclei, proton nuclei, and unpaired electrons (from TaS_2), brought about by dynamical motion. In most polymer electrolytes

Figure 12. Temperature dependence of line-width as a function of (A) T and (B) $1/T$ of ^{7}Li NMR resonance peaks for (a) $Li_{0.2}TaS_2$ and (b) $Li_{0.2}(PEO)_{1.04}TaS_2$ (batch II; MW $\sim$ 100 000).

Table 4. Effect of Film Orientation on the ^{7}Li NMR Spectrum of $Li_{0.2}(PEO)_yTaS_2$[a]

	$Li_{0.2}(PEO)_yTaS_2$ (batch I)		$Li_{0.2}(PEO)_yTaS_2$ (batch II)	
	parallel	perpendicular	parallel	perpendicular
chemical shift of peak position (ppm)	3.14	12.57	10.99	9.42
line-width (Hz)	2893	4618	2924	2902

[a] "Parallel" and "perpendicular" refer to the film with respect to the instrument's applied magnetic field.
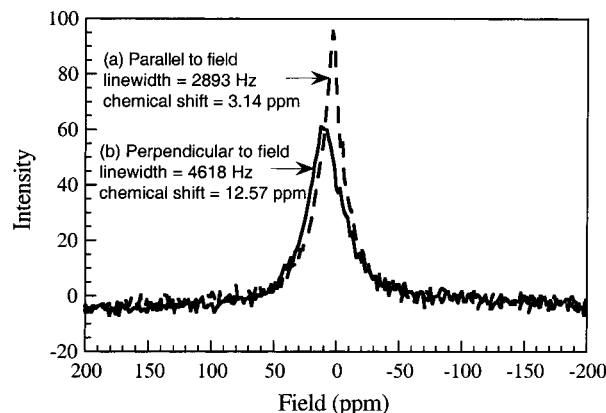

Figure 13. Room temperature ^{7}Li NMR spectra for a $Li_{0.2}$-$(PEO)_{1.04}TaS_2$ film (batch I; MW $\sim$ 100 000): (a) film parallel to the magnetic field and (b) film perpendicular to the field.

and PEO nanocomposites, such motional narrowing is caused by dissociation of dipole−dipole coupling between pairs of nuclear spins, specifically, ^{7}Li$^+$ and ^{1}H$^+$ of the PEO.[40−42] It reflects the onset of the dynamical motion of the polymer chains and or the Li$^+$ ions. In some materials with unpaired electrons the line narrowing is caused mainly by averaging over the dipole couplings in the electron spin field, because the electrons produce much larger spin fields than nuclei.[42]

$Li_{0.2}(PEO)_yTaS_2$ is similar to Li/PEO/fluorohectorite,[42b] a nanocomposite without paramagnetic centers. One might expect that the broadening of the ^{7}Li resonance peak results mainly from the dipole−dipole coupling between ^{7}Li and ^{1}H of the PEO, as in the case of Li/PEO/fluorohectorite.[41b] This assignment would be supported by the similar line-widths before narrowing in these two nanocomposites, $\sim$5 kHz, and the appearance of the plateau on the low-temperature as well as high-temperature side. If this is the case, the dynamical motional narrowing should correspond to the onset of the segmental motion of the polymer chains. However, the temperature range of the narrowing, −40 to 60 °C, is closer to the onset temperature of Li$^+$ ion motion observed in Li/PEO/montmorillonite, −20 to 40 °C,[41a,b] rather than that of the polymer segmental motion observed in Li/PEO/fluorohectorite, −100 to 40 °C.[41b] In

(42) (a) Savariault J. M., Deramond E., Galy J., Mongrelet T., Hirschinger J. *Mol. Cryst. Liq. Cryst.* **1994**, *244*: 367 (b) Hirschinger J., Mongrelet T., Marichal C., Granger P., Savariault J. M., Deramond E, Galy J. *J. Phys. Chem.* **1993**, *97*, 10301. (c) Cocciantelli Jm, Suh Ks, Senegas J., Doumerc J. P., Pouchard M. *J Phys Chem Solids* **1992**, *53*, 57.

LiClO$_4$(PEG)$_9$ and LiBF$_4$(PEG)$_9$, where the motion of Li$^+$ ions is essentially governed by segmental motion of the polymer chains and the line narrowing corresponds to both the onset of the correlated motions of Li$^+$ ions and polymer segments, the narrowing occurs in the range of −50 to 50 °C.[39a] Because the line narrowing in $Li_{0.2}$-TaS_2 and $Li_{0.2}(PEO)_yTaS_2$ happens in the same temperature range, it is possible that the dynamical motional narrowing observed in $Li_{0.2}(PEO)_yTaS_2$ is caused by the onset of Li$^+$ ion hopping in the gallery. This is reasonable, since the $[TaS_2]^{x-}$ anions are massive and only the motion of Li$^+$ ions is conceivable. On the other hand, after narrowing, the line-width is much wider in $Li_{0.2}$-$(PEO)_yTaS_2$ ($\sim$1500 Hz) than in LiClO$_4$(PEG)$_9$ and LiBF$_4$(PEG)$_9$ (60−90 Hz). This suggests that the broadening of the ^{7}Li resonance peak in $Li_{0.2}(PEO)_yTaS_2$ is not caused only by the dipole−dipole coupling between ^{7}Li and the polymer protons. For comparison with literature data, the ^{7}Li NMR line-widths of $Li_{0.2}TaS_2$ and $Li_{0.2}(PEO)_yTaS_2$ are plotted against $1/T$ in Figure 12B.

The considerable narrowing of the ^{7}Li resonance peak of $Li_{0.2}(PEO)_yTaS_2$ at high temperatures suggests that the lithium ions begin to undergo facile site hopping. The mobility of lithium ions is affected by temperature more readily in the polymer-intercalated galleries than in the $Li_{0.2}TaS_2$ galleries. This is attributed to the more disordered environment of the Li sites in the nanocomposites, which lowers the activation barrier for hopping, as opposed to the more ordered, crystallographically better defined sites in $Li_{0.2}TaS_2$. The narrowing of linewidth in ^{7}Li NMR spectra has also been observed in $Li_xV_2O_5$[42] and Li_xMoO_3[4b] as well as their PEO nanocomposites.

A high degree of anisotropy was observed in the solid-state ^{7}Li NMR spectra of $Li_{0.2}(PEO)_yTaS_2$ films (both

batches I and II). The results of these experiments are summarized in Table 4. As shown in Figure 13, in batch I both the resonance peak position and peak-width vary with the change in film orientation relative to the direction of applied magnetic field. When the film is oriented perpendicular to the field, the peak width is broadened considerably more than when it is parallel. The reason for this is not yet clear; however, the highly mobile electrons in the two-dimensional TaS$_2$ slabs probably couple to the external applied magnetic field and cause local field distortions, which influence the ^{7}Li NMR signals. This orientation effect is there but less pronounced in films of batch II Li$_{0.2}$(PEO)$_y$TaS$_2$, probably due to the fact that the slabs of TaS$_2$ are smaller, less well stacked, and more separated by PEO molecules.

Concluding Remarks

The exfoliation properties of Li$_x$TaS$_2$ were systematically explored and it was found that samples prepared from controlled lithiation with 0.2 equiv of LiBH$_4$, exfoliate well in water and have high affinity for various polymers. Lamellar nanocomposites of PEO, PEI, and PVP were thus obtained through the encapsulative precipitation method. The nanocomposites suspend in water and are easily cast into films that can be peeled off as free-standing. These plastic-like films become superconductors at temperatures below their T_c value, which raises the possibility of developing flexible superconductors with these or other materials for specific applications. Analysis of the X-ray diffraction data for Li$_x$(PEO)$_y$TaS$_2$ suggests that the nanocomposites are constructed with two sheets of PEO chains (bilayer) inserted in each gallery. The PEO chains adopt a conformation similar to that found in type II PEO–HgCl$_2$ complex and are arranged with the $-$CH$_2-$ groups facing the TaS$_2$ layers and the $-$O$-$ atoms toward the center of the gallery, where the Li$^+$ ions seem to be located. Solid-state ^{7}Li NMR measurements indicate that Li$_x$(PEO)$_y$TaS$_2$ provides a more facile hopping environment for Li ions than does Li$_x$TaS$_2$.